# A HYBRID METHOD FOR SYSTEMS OF CLOSELY SPACED DIELECTRIC SPHERES AND IONS*

ZECHENG GAN†, SHIDONG JIANG‡, ERIK LUIJTEN§, AND ZHENLI XU¶

**Abstract.** We develop an efficient, semianalytical, spectrally accurate, and well-conditioned hybrid method for the study of electrostatic fields in composites consisting of an arbitrary distribution of dielectric spheres and ions that are loosely or densely (close to touching) packed. We first derive a closed-form formula for the image potential of a general multipole source of arbitrary order outside a dielectric sphere. Based on this formula, a hybrid method is then constructed to solve the boundary value problem by combining these analytical methods of image charges and image multipoles with the spectrally accurate mesh-free method of moments. The resulting linear system is well conditioned and requires many fewer unknowns on material interfaces as compared with standard boundary integral equation methods, in which the formulation becomes increasingly ill-conditioned and the number of unknowns also increases sharply as the spheres approach each other or ions approach the spheres due to the geometric and physical stiffness. We further apply the fast multipole method to accelerate the calculation of charge–charge, charge–multipole, and multipole–multipole interactions to achieve optimal computational complexity. The accuracy and efficiency of the scheme are demonstrated via several numerical examples.

**Key words.** fast algorithm, dielectric spheres, Poisson equation, self-assembly

**AMS subject classifications.** 31B05, 35Q82, 65N80, 78M16

**DOI.** 10.1137/15M105046X

**1. Introduction.** Electrostatic interactions arise in many areas of science and engineering, from the surface tension of cloud droplets to protein folding, and from soft-matter physics and environmental science to electrical engineering [1, 2]. Their long-range nature makes efficient algorithms for electrostatic problems, which are described by the Poisson equation, of paramount importance. Indeed, various methods have been developed for the solution of the Poisson equation for different systems. If the dielectric function $\epsilon(\mathbf{r})$ is a general space-dependent function, the Poisson equation is often solved by grid-based finite-difference or finite-element methods accelerated by

multigrid algorithms. However, these methods are generally less efficient for molecular dynamics or Monte Carlo simulations of charged objects embedded in an inhomogeneous medium. One class of systems that has generated particularly widespread attention is that of suspensions of spherical colloids, which serve as model systems in self-assembly [3, 4] and also find broad applications in biology and physical chemistry [5]. For such specific dielectric functions, numerical methods for electrostatic problems can be very efficient.

Here we consider the solution of the Poisson equation for a model system consisting of $M$ dielectric spheres $S_j$ $(j = 1, \ldots, M)$ of radius $a_j$, with the $j$th sphere centered at $\mathbf{o}_j$; this is schematically shown in Figure 1. We further assume that the spheres are neither touching nor intersecting, i.e., $S_i \bigcap S_j = \varnothing$. The domain $\mathbb{R}^3$ is then divided into an interior region, $\Omega = \bigcup\{S_j, j = 1, \ldots, M\}$, and an exterior region, $\Omega^c = \mathbb{R}^3 \backslash \Omega$. The dielectric permittivity $\epsilon(\mathbf{r})$ is assumed to be constant inside each sphere and within the surrounding medium, i.e.,

$$(1) \qquad \epsilon(\mathbf{r}) = \begin{cases} \epsilon_j & \text{for } \mathbf{r} \in S_j,\ j = 1, \ldots, M\ , \\ \epsilon_s & \text{for } \mathbf{r} \in \Omega^c\ , \end{cases}$$

where $\epsilon_j$ is the permittivity of the $j$th sphere, and $\epsilon_s$ is the permittivity of the surrounding medium. We also assume that $N$ point source charges of strength $q_i$ located at $\mathbf{r}_i \in \Omega^c$, $i = 1, \ldots, N$, are embedded in the surrounding medium, which represent small ions in the system. The electrostatic potential $\Phi(\mathbf{r})$ of the system is then governed by the Poisson equation,

$$(2) \qquad \begin{cases} \nabla^2 \Phi(\mathbf{r}) &= 0 & \text{for } \mathbf{r} \in \Omega\ , \\ -\nabla^2 \Phi(\mathbf{r}) &= \rho(\mathbf{r})/\epsilon_s & \text{for } \mathbf{r} \in \Omega^c\ , \end{cases}$$

where $\rho(\mathbf{r}) = \sum_{i=1}^{N} q_i \delta(\mathbf{r} - \mathbf{r}_i)$ is the source charge distribution in the exterior region, and $\delta(\cdot)$ denotes the Dirac delta function. On the interfaces between the spheres and the surrounding medium we have standard electrostatic boundary conditions to describe the continuities of the electric potential and the electric displacement [6], i.e.,

$$(3) \qquad \Phi(\mathbf{r}^-) = \Phi(\mathbf{r}^+)\ ,$$

$$(4) \qquad \epsilon_j \frac{\partial \Phi(\mathbf{r}^-)}{\partial \mathbf{n}} = \epsilon_s \frac{\partial \Phi(\mathbf{r}^+)}{\partial \mathbf{n}}$$

for $\mathbf{r} \in \partial S_j$, $j = 1, 2, \ldots, M$. Here $\mathbf{r}^-$ and $\mathbf{r}^+$ are the inner and outer limits at position $\mathbf{r}$, and $\mathbf{n}$ is the outward unit vector normal to the interface.

In cases with sharp dielectric interfaces (i.e., the dielectric permittivity is piecewise constant), the boundary integral equation (BIE) method has become a standard and popular approach [7, 8, 9]. The advantage of the BIE method is that it chooses the representation that satisfies the Poisson equation in the bulk, and one only needs to solve a system of integral equations on the material interfaces, thus reducing the dimension of the problem by one. When combined with fast algorithms such as the fast multipole method (FMM) [10, 11, 12], the BIE approach achieves optimal complexity. Obviously, our problem is a special case of this general class, and the BIE approach is applicable to our problem.

Another popular method that takes advantage of the spherical geometry is the method of moments (MoM) [13, 14, 15, 16, 17]. Here the electric potential inside each sphere is expressed as a local spherical harmonic expansion of order $p$, whereas the electric potential outside the spheres is expressed as the sum of a multipole spherical harmonic expansion of a certain order on each sphere and the potential due to
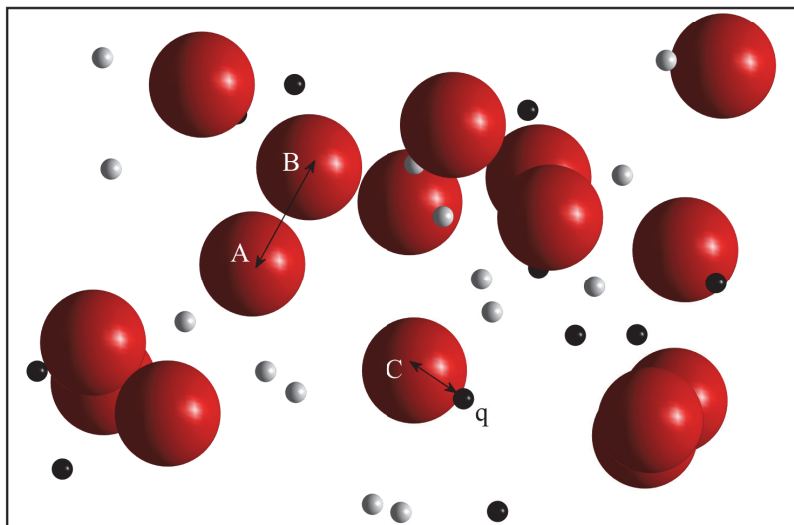
FIG. 1. *Schematic illustration of a system of dielectric spheres and ions. In the hybrid scheme (for details see section 4), when an ion is close to a sphere (e.g., q is close to sphere C), the contribution of its image charges is added to the spherical harmonic expansion. When dielectric spheres are close to each other (e.g., spheres A and B), the image potential of multipoles is used.*

each point charge. Applying standard multipole-to-local (M2L) and particle-to-local (P2L) operations in the FMM, the boundary conditions lead to a linear system of size $O(Mp^2)$ which may be solved iteratively using the generalized minimum residual (GMRES) method [18]. The advantage of the MoM, as compared with the BIE approach, is that it avoids the quadrature discretization part of the BIE approach. The standard quadrature for weakly singular integrals (with $\frac{1}{r}$ singularity) [19] is usually of low order on a triangular mesh for most practical applications. The quadrature developed in [20], which can integrate weakly singular integrals to high order for a closed smooth surface homeomorphic to a sphere, has $O(p^4 \log p)$ complexity. Recently, the so-called quadrature-by-expansion (QBX) scheme [21, 22, 23] has become an area of extensive study and development. This scheme can evaluate layer potentials to high accuracy and is easily coupled with the FMM. We expect that the FMM-accelerated QBX scheme will have a great impact on the BIE approach for solving three-dimensional problems in the near future.

However, when spheres and ions are densely packed in a medium, the induced charge density on each sphere will be sharply peaked at the point where two spheres are nearly touching or an ion is very close to a sphere. In this case, both the BIE formulation and the MoM will suffer from ill-conditioning due to the dense geometry [24, 25]. Indeed, even if the BIE formulation is of the second kind, the condition number of the BIE formulation increases as the spheres are getting closer and closer to each other, and it becomes more difficult to design adaptive meshes and high-order quadratures. Likewise, for the MoM the order $p$ of the spherical harmonic expansion needed to achieve a certain accuracy increases dramatically as spheres are close to touching or the ions are very close to the spheres, making the method impractical.

On the other hand, we observe that the method of image charges can be applied to solve the problem analytically when the system contains only one sphere. This method introduces fictitious mirror charges, placed at the opposite side of the

interface, to satisfy boundary conditions on the interface [26, 27, 28, 29]. The image-charge representations for the polarization potential induced by a point charge near a *conducting plane* or *sphere* are well known in two and three dimensions [6]. For a conducting sphere, the exact image rule for an *arbitrary-order multipole source* is known as well [30]. For a *dielectric sphere*, the corresponding image-charge formula is more complicated, namely a point charge plus a line charge density distributed from the sphere center to the Kelvin point [27]. The image for a *dipole source* near a *dielectric sphere* was found by Lindell [31] as a superposition of point charges, point dipoles, line charges, and line dipoles. However, the image rule for a *general multipole source* near a *dielectric sphere* does not seem to be available in the literature. Moreover, the method of image charges becomes very clumsy and impractical when the system contains many spheres owing to multiple scattering (cf. [32, 33] for a detailed discussion of this point).

In this paper, we derive the images of a general multipole source near a dielectric sphere. This allows us to develop a hybrid method for the evaluation of the electrostatic field in composites consisting of arbitrarily packed dielectric spheres and ions. The basic idea of this hybrid method is as follows. If the spheres and ions are well separated, the MoM is coupled with the FMM and an iterative solver to take advantage of the spherical geometry and achieve optimal complexity. If ions are close to a sphere, we add the effect of the image charges directly into the electric potential and the electric field both inside and outside the sphere. This greatly reduces the order of the spherical harmonic expansions. Finally, if spheres are close to each other, we modify the linear system to take into account the effect of the image multipole expansions. This effectively reduces the ill-conditioning of the problem and also significantly lowers the order of the spherical harmonic expansions. Our work is a natural extension of earlier work on conducting spheres [24]. However, in addition, we have modified the FMM to accelerate the calculation of interactions between multipole/local expansions on spheres. The overall scheme eliminates the most "singular" part of the electric potential, effectively reduces the ill-conditioning of the system due to close-to-touching geometries, reduces the total number of unknowns by lowering the order of the spherical harmonic expansion by a large factor, and achieves optimal complexity of the GMRES iteration through use of the FMM. This will enable particle simulations of large-scale systems, such as the equilibrium properties of dielectric nanoparticle self-assembly [4].

This paper is organized as follows. In section 2, we collect some known results about spherical harmonic expansions. In section 3, we derive the images of a *general multipole source* near a *dielectric sphere*. In section 4, we present the hybrid scheme for the rapid evaluation of electrostatic potentials and fields for a composite consisting of arbitrarily packed spheres and ions. The performance of the scheme is illustrated via several numerical examples in section 5. We end with a short discussion in section 6.

**2. Mathematical preliminaries.** We first review mathematical preliminaries on spherical harmonics [6, 34, 35, 36, 37], which will subsequently be used in the presentation of our algorithm. To simplify the notation, we denote the infinite summation $\sum_{n=0}^{+\infty} \sum_{m=-n}^{n}$ by $\sum_{n,m}$ and the truncated $p$th-order spherical harmonic expansion $\sum_{n=0}^{p} \sum_{m=-n}^{n}$ by $\sum_{n,m}^{p}$. We start with the definition of the spherical harmonics.

DEFINITION 1. *The spherical harmonic of degree n and order m is defined by*

$$(5) \qquad Y_n^m(\theta, \varphi) = \sqrt{\frac{(n-|m|)!}{(n+|m|)!}} \cdot P_n^{|m|}(\cos\theta) e^{im\varphi} \quad \text{for } n \geq 0 \text{ and } |m| \leq n ,$$

where $\theta$ and $\varphi$ represent colatitude and longitude angles, respectively. $P_n^m$ is the associated Legendre function, defined by Rodrigues's formula,

$$(6) \qquad P_n^m(x) = (-1)^m (1-x^2)^{m/2} \frac{d^m}{dx^m} P_n(x) \ ,$$

with $P_n(x)$ the Legendre polynomial of degree $n$.

The following multipole expansion is used to represent the far field outside a sphere containing a cluster of source charges; its truncation results in an efficient low-rank approximation for the field in the region that is well separated from the source sphere.

LEMMA 2 (multipole expansion). *Suppose $N$ point charges of strengths $\{q_i, i = 1, \ldots, N\}$ are located at $\{\mathbf{r}_i = (\rho_i, \alpha_i, \beta_i), i = 1, \ldots, N\}$ in spherical coordinates. Suppose the charges are all within a sphere of radius $a$ centered at the origin. Then, for any point $\mathbf{r} = (r, \theta, \varphi)$ with $r > a$, the potential $\Phi(\mathbf{r})$ can be expressed as a multipole expansion,*

$$(7) \qquad \Phi(\mathbf{r}) = \sum_{n,m} \frac{M_n^m}{r^{n+1}} Y_n^m(\theta, \varphi) \ ,$$

*with coefficients*

$$(8) \qquad M_n^m = \sum_{i=1}^{N} q_i \rho_i^n Y_n^{-m}(\alpha_i, \beta_i) \ .$$

Alternatively, if all the target points are located in a sphere away from the sources, the following local expansion may be used to represent the field in the target sphere; its finite-order truncation results in an efficient low-rank approximation for the field when the sources are well separated from the target sphere.

LEMMA 3 (local expansion). *Suppose $N$ point charges of strengths $\{q_i, i = 1, \ldots, N\}$ are located at $\{\mathbf{r}_i = (\rho_i, \alpha_i, \beta_i), i = 1, \ldots, N\}$ in spherical coordinates. Suppose the charges are all located outside a sphere of radius $a$ centered at the origin. Then, for any point $\mathbf{r} = (r, \theta, \varphi)$ with $r < a$, the potential $\Phi(\mathbf{r})$ can be expanded as a local expansion,*

$$(9) \qquad \Phi(\mathbf{r}) = \sum_{n,m} L_n^m r^n Y_n^m(\theta, \varphi) \ ,$$

*where*

$$(10) \qquad L_n^m = \sum_{i=1}^{N} q_i \frac{Y_n^{-m}(\alpha_i, \beta_i)}{\rho_i^{n+1}} \ .$$

The induced charge due to a point source charge outside a dielectric sphere can be expressed by the Neumann image principle [27, pp. 279–282] (for more discussion, see also [28, 29]). We will use this formulation to treat the singularity when charges are close to a spherical interface. We note that when the source charge is located inside the dielectric sphere, the image structure can be derived in a very similar fashion (see, e.g., [38]).

THEOREM 4 (Neumann image principle for single sphere). *Suppose that $S$ is a dielectric sphere of radius $a$ and with dielectric constant $\epsilon_1$, centered at the origin $\mathbf{o} = (0,0,0)$ and surrounded by a uniform medium with dielectric constant $\epsilon_s$. Suppose further that a source charge $q$ is located at $\mathbf{r}' = (r', \theta', \varphi')$ outside the sphere, i.e., $r' > a$. Then the induced electrostatic potential at any point $\mathbf{r}$ inside or outside the sphere can be represented by the superposition of the potentials due to a point and a line image charge, that is,*

$$(11) \qquad \Phi(\mathbf{r}) = \begin{cases} \dfrac{q_{\text{in}}}{4\pi\epsilon_s|\mathbf{r}-\mathbf{r}'|} + \displaystyle\int_{r'}^{\infty} \dfrac{Q_{\text{in}}(x)}{4\pi\epsilon_s|\mathbf{r}-\mathbf{x}|}dx\,, & \mathbf{r} \in S\,, \\[4mm] \dfrac{q}{4\pi\epsilon_s|\mathbf{r}-\mathbf{r}'|} + \dfrac{q_{\text{K}}}{4\pi\epsilon_s|\mathbf{r}-\mathbf{r}_{\text{K}}|} + \displaystyle\int_{0}^{r_{\text{K}}} \dfrac{Q_{\text{out}}(x)}{4\pi\epsilon_s|\mathbf{r}-\mathbf{x}|}dx\,, & \mathbf{r} \in S^c\,, \end{cases}$$

*where $\mathbf{x} = x\mathbf{r}'/r'$, the position of Kelvin image charge $\mathbf{r}_{\text{K}} = \mathbf{r}' a^2 / r'^2$, and the strengths of the point and line image charges for interior and exterior fields are, respectively,*

$$(12) \qquad \begin{cases} q_{\text{in}} = 2\lambda q\,, \quad Q_{\text{in}}(x) = \dfrac{\gamma\lambda q}{r'}\left(\dfrac{r'}{x}\right)^{\lambda}\,, \\[4mm] q_{\text{K}} = -\dfrac{\gamma a q}{r'}\,, \quad Q_{\text{out}}(x) = \dfrac{\gamma\lambda q}{a}\left(\dfrac{r_{\text{K}}}{x}\right)^{1-\lambda}\,. \end{cases}$$

*Here $\gamma = (\epsilon_1 - \epsilon_s)/(\epsilon_1 + \epsilon_s)$ and $\lambda = \epsilon_s/(\epsilon_1 + \epsilon_s)$ are constants.*

**3. Image potentials for a multipole source.** In this section, we consider the image potentials of a general multipole source outside a dielectric sphere. We will extend the Neumann image principle, Theorem 4, to treat a multipole source, which results in a generalized image-charge method (GICM).

DEFINITION 5. *For $\mathbf{r} \neq \mathbf{c}$, a multipole source of order $n$ and degree $m$ $(n \geq |m|)$ at position $\mathbf{c}$ is defined by*

$$(13) \qquad \Phi_0(\mathbf{r}) = \frac{M_n^m}{r_c^{n+1}}Y_n^m(\theta_c, \varphi_c)\,,$$

*where the coefficient $M_n^m$ describes the strength of the multipole source and $(r_c, \theta_c, \varphi_c) = \mathbf{r} - \mathbf{c}$ are spherical coordinates. If $n = |m|$, we call the multipole source a sectoral multipole of order $n$.*

Assume that a dielectric sphere $S$ of radius $a$ is centered at the origin $\mathbf{o}$ and a multipole source $\Phi_0(\mathbf{r})$ is located outside the sphere. We will derive image representations as closed-form solutions for induced potentials. We first study a special and simple case: a unit sectoral multipole $\Phi_0(\mathbf{r})$, i.e., $M_n^m = 1$ and $n = |m|$ in (13), placed on the $+z$-axis. The following theorem gives a simple and direct formula for the image potentials $\Psi(\mathbf{r})$ and $\Phi(\mathbf{r})$. This is an extension of the result for a conducting sphere [24], where the interface conditions are reduced to a single Dirichlet boundary condition.

THEOREM 6 (image potentials for a sectoral multipole). *Suppose $S$ is a dielectric sphere of radius $a$ centered at the origin with permittivity $\epsilon_1$ and surrounded by a uniform medium with permittivity $\epsilon_s$. Let $\Phi_0(\mathbf{r})$ be a unit sectoral multipole of order $k$ at $\mathbf{c} = (0,0,h)$ (in Cartesian coordinates) with $h > a$,*

$$(14) \qquad \Phi_0(\mathbf{r}) = \frac{1}{r_c^{k+1}}Y_k^k(\theta_c, \varphi_c)\,.$$

*Then the induced potentials outside and inside S are*

$$(15) \qquad \Psi(\mathbf{r}) = \frac{C_k}{r_g^{k+1}} Y_k^k(\theta_g, \varphi_g) - \frac{\lambda C_k}{r_K} \int_0^{r_K} \frac{(r_K/x)^{1-\lambda-k}}{r_x^{k+1}} Y_k^k(\theta_x, \varphi_x) dx \ ,$$

$$(16) \qquad \Phi(\mathbf{r}) = \frac{1-\gamma}{r_c^{k+1}} Y_k^k(\theta_c, \varphi_c) + \frac{\lambda \gamma}{h} \int_h^\infty \frac{(h/x)^{\lambda-k}}{r_x^{k+1}} Y_k^k(\theta_x, \varphi_x) dx \ ,$$

*respectively. Here* $\gamma = (\epsilon_1 - \epsilon_s)/(\epsilon_1 + \epsilon_s)$, $\lambda = \epsilon_s/(\epsilon_1 + \epsilon_s)$, $r_K = a^2/h$, *the coefficient* $C_k$ *is*

$$(17) \qquad C_k = (-1)^{k+1} \gamma \left(\frac{a}{h}\right)^{2k+1} \ ,$$

$(r_g, \theta_g, \varphi_g)$ *and* $(r_x, \theta_x, \varphi_x)$ *are the spherical coordinates of* $\mathbf{r} - \mathbf{r}_K$ *and* $\mathbf{r} - \mathbf{x}$, *respectively, and* $\mathbf{r}_K$ *and* $\mathbf{x}$ *are on the ray of* $\mathbf{c}$,

$$(18) \qquad \mathbf{r}_K = (r_K, 0, 0) = \frac{a^2}{h^2}\mathbf{c} \ \ and \ \mathbf{x} = (x, 0, 0) \ .$$

*Proof.* We first expand $\Phi_0(\mathbf{r})$ into a local expansion centered at the origin [24],

$$(19) \qquad \Phi_0(\mathbf{r}) = (-1)^k \sum_{n=k}^\infty \sqrt{\binom{n+k}{2k}} \frac{r^n}{h^{n+k+1}} Y_n^k(\theta, \varphi) \ .$$

Since $\Psi$ outside $S$ and $\Phi$ inside $S$ are both harmonic, they can be expressed in terms of harmonic series with unknown coefficients $A_n$ and $B_n$,

$$(20) \qquad \Psi(\mathbf{r}) = \sum_{n=k}^\infty \frac{A_n}{r^{n+1}} Y_n^k(\theta, \varphi) \ , \quad \mathbf{r} \in S^c \ ,$$

$$(21) \qquad \Phi(\mathbf{r}) = \sum_{n=k}^\infty B_n r^n Y_n^k(\theta, \varphi), \quad \mathbf{r} \in S \ .$$

The boundary conditions at $r = a$ are $\Phi_0 + \Psi = \Phi$ and $\epsilon_s \frac{\partial(\Phi_0+\Psi)}{\partial r} = \epsilon_1 \frac{\partial \Phi}{\partial r}$. Substituting (19)–(21) into these boundary conditions and using the orthogonality of spherical harmonics, we obtain a $2 \times 2$ system for $A_n$ and $B_n$, for each $n$. Solving this system yields

$$(22) \qquad \begin{aligned} A_n &= (-1)^k \left[ -\gamma + \frac{\gamma(1-\gamma)}{1-\gamma+2n} \right] \sqrt{\binom{n+k}{2k}} \frac{a^{2n+1}}{h^{n+k+1}} \ , \\ B_n &= (-1)^k \frac{(1-\gamma)(2n+1)}{1-\gamma+2n} \sqrt{\binom{n+k}{2k}} \frac{1}{h^{n+k+1}} \ . \end{aligned}$$

Substituting $A_n$ into (20), we observe that $\Psi(\mathbf{r})$ can be written as the sum of two terms,

$$(23) \qquad \Psi(\mathbf{r}) = \Psi_1(\mathbf{r}) + \Psi_2(\mathbf{r}),$$

where

$$(24) \qquad \Psi_1(\mathbf{r}) = (-1)^{k+1} \gamma \sum_{n=k}^\infty \left[ \sqrt{\binom{n+k}{2k}} \frac{a^{2n+1}}{h^{n+k+1}} \right] \frac{Y_n^k(\theta, \varphi)}{r^{n+1}} \ ,$$

$$(25) \qquad \Psi_2(\mathbf{r}) = (-1)^k \sum_{n=k}^\infty \left[ \frac{\gamma(1-\gamma)}{1-\gamma+2n} \sqrt{\binom{n+k}{2k}} \frac{a^{2n+1}}{h^{n+k+1}} \right] \frac{Y_n^k(\theta, \varphi)}{r^{n+1}} \ .$$

Applying an identity similar to (19) in the reverse direction, we observe that $\Psi_1(\mathbf{r})$ is the expansion of an image sectoral multipole at $\mathbf{r}_K$. Thus,

$$(26) \qquad \Psi_1(\mathbf{r}) = \frac{C_k}{r_g^{k+1}} Y_k^k(\theta_g, \varphi_g) .$$

For $\Psi_2(\mathbf{r})$, we introduce the following identity:

$$(27) \qquad \int_0^b \frac{1}{x} \left(\frac{x}{b}\right)^{\frac{1}{2}(1-\gamma+2n)} dx = \frac{2}{1-\gamma+2n} .$$

Using this identity with $b = r_K$ in (25) and an identity similar to (19), we obtain

$$(28) \qquad \Psi_2(\mathbf{r}) = -\frac{\lambda C_k}{r_K} \int_0^{r_K} \frac{(r_K/x)^{1-\lambda-k}}{r_x^{k+1}} Y_k^k(\theta_x, \varphi_x) dx ,$$

and (15) follows. Since the expression (16) for the induced potential inside the sphere can be obtained in an almost identical manner, we omit the details. $\square$

*Remark* 7. We make two observations. First, the image potential for the other sectoral multipole $Y_k^{-k}(\theta_c, \phi_c)/r_c^{k+1}$ can be obtained directly, since it is the complex conjugate of $Y_k^k$; second, when $k = 0$, (15) and (16) recover the classic Neumann image formula of Theorem 4, where the image point multipole and line multipole reduce to point and line charges, respectively.

The following differential relation connects a general multipole with the sectoral multipole [30].

LEMMA 8 (differential relation). *Consider a general multipole*

$$(29) \qquad \Theta_l^k(\mathbf{r}) = \frac{Y_l^k(\theta, \varphi)}{r^{l+1}} ,$$

*where $(r, \theta, \varphi)$ are the spherical coordinates of $\mathbf{r}$. Then*

$$(30) \qquad \Theta_l^k(\mathbf{r} - h\mathbf{n}) = G_l^k \cdot \frac{\partial^{l-k}}{\partial h^{l-k}} \Theta_k^k(\mathbf{r} - h\mathbf{n}) ,$$

*where $\mathbf{n} = (0, 0, 1)$ is the unit vector along the $+z$-axis and*

$$(31) \qquad G_l^k = \sqrt{\frac{(2k)!}{(l+k)!(l-k)!}} .$$

The following identity, which generalizes the chain rule to higher-order derivatives [39], is also needed in deriving the image potentials for a general multipole source.

LEMMA 9 (Faà di Bruno's formula). *If $g(t)$ and $f(t)$ are functions of $t$ with a sufficient number of derivatives, then*

$$(32) \qquad \frac{d^m}{dt^m} g(f(t)) = \sum_{k=1}^m g^{(k)}(f) \cdot B_{m,k}(f', f'', \ldots, f^{(m-k+1)}) .$$

*Here $B_{m,k}$ are Bell polynomials,*

$$(33) \quad B_{m,k}(x_1, x_2, \cdots, x_{m-k+1})$$
$$= \sum \frac{m!}{c_1! c_2! \cdots c_{m-k+1}!} \left(\frac{x_1}{1!}\right)^{c_1} \left(\frac{x_2}{2!}\right)^{c_2} \cdots \left(\frac{x_{m-k+1}}{(m-k+1)!}\right)^{c_{m-k+1}} ,$$

*where the sum is taken over all nonnegative integers $\{c_i, \ i = 1, \ldots, m - k + 1\}$ that satisfy the constraints*

$$\sum_{i=1}^{m-k+1} c_i = k \ , \qquad \sum_{i=1}^{m-k+1} i c_i = m \ .$$

*In particular, when $x_i = i!, \ i = 1, \ldots, m - k + 1$,*

(34) $$B_{m,k}(x_1, x_2, \ldots, x_{m-k+1}) = \left( \begin{array}{c} m \\ k \end{array} \right) \left( \begin{array}{c} m - 1 \\ k - 1 \end{array} \right) (m - k)! \ .$$

We are now in a position to state our main analytical result, namely a closed-form solution of image potentials for a general multipole source outside a dielectric sphere.

THEOREM 10 (image potentials for a general multipole). *Suppose $S$ is a dielectric sphere of radius $a$ centered at the origin with permittivity $\epsilon_1$ and surrounded by a uniform medium with permittivity $\epsilon_s$. Let $\Phi_0$ be a unit multipole source of general order and degree at $\mathbf{c} = (0, 0, h)$ (in Cartesian coordinates) with $h > a$,*

(35) $$\Phi_0(\mathbf{r}) = \frac{1}{r_c^{l+1}} Y_l^k(\theta_c, \varphi_c) \ , \quad l \geq k \ .$$

*Then the induced potentials outside and inside $S$ are*

(36) $$\Psi(\mathbf{r}) = \sum_{j=k}^{l} N_{lj}^k \left[ \frac{1}{r_g^{j+1}} Y_j^k(\theta_g, \varphi_g) - \frac{\lambda}{r_K} \int_0^{r_K} \frac{(r_K/x)^{1-\lambda-j}}{r_x^{j+1}} Y_j^k(\theta_x, \varphi_x) dx \right] \ ,$$

(37) $$\Phi(\mathbf{r}) = \frac{(1 - \gamma)}{r_c^{l+1}} Y_l^k(\theta_c, \varphi_c) + \frac{\lambda\gamma}{h} \int_h^\infty \frac{(h/x)^{\lambda-l}}{r_x^{l+1}} Y_l^k(\theta_x, \varphi_x) dx \ ,$$

*respectively. Here $\lambda, \gamma, r_K, (r_g, \theta_g, \varphi_g)$, and $(r_x, \theta_x, \varphi_x)$ are the same as in Theorem 6, and the coefficients $N_{lj}^k \ (j = k, \ldots, l)$ are defined by*

(38)

$$\begin{cases} N_{lk}^k = (-1)^{l+1} \gamma \dfrac{(l+k)!}{(2k)!} \dfrac{a^{2k+1}}{h^{l+k+1}} G_l^k \ , \\[2ex] N_{lj}^k = (-1)^{l+1} \gamma \dfrac{a^{2j+1}}{h^{l+j+1}} \sqrt{\dfrac{(j+k)!(j-k)!}{(2k)!}} G_l^k \\[2ex] \qquad \cdot \displaystyle\sum_{i=j-k}^{l-k} \dfrac{(l+k-i)!(i-j+k)!}{(2k)!} \left( \begin{array}{c} l-k \\ i \end{array} \right) \left( \begin{array}{c} i \\ j-k \end{array} \right) \left( \begin{array}{c} i-1 \\ j-k-1 \end{array} \right) \ , \\[2ex] \qquad j = k+1, \ldots, l \ . \end{cases}$$

*Proof.* Let $\mathbf{n} = (0, 0, 1)$. Clearly, $\Phi_0(\mathbf{r}) = \Theta_l^k(\mathbf{r} - h\mathbf{n})$. Applying Lemma 8, we may express the general multipole source in terms of the derivative of a sectoral multipole,

(39) $$\Phi_0(\mathbf{r}) = G_l^k \frac{\partial^{l-k}}{\partial h^{l-k}} \Theta_k^k(\mathbf{r} - h\mathbf{n}) \ .$$

The induced potential for the sectoral multipole source $\Theta_k^k(\mathbf{r} - h\mathbf{n})$ has already been obtained in Theorem 6. By linearity and (39), the induced potential of the general multipole is simply the derivative of the induced potential of the sectoral multipole source. Thus, the induced potential outside the sphere is

(40) $$\Psi(\mathbf{r}) = \Psi_1(\mathbf{r}) + \Psi_2(\mathbf{r}),$$

where

$$(41) \quad \Psi_1(\mathbf{r}) = (-1)^{k+1} \gamma G_l^k \cdot \frac{\partial^{l-k}}{\partial h^{l-k}} \left\{ \left(\frac{a}{h}\right)^{2k+1} \frac{1}{r_g^{k+1}} Y_k^k(\theta_g, \varphi_g) \right\} ,$$

$$(42) \quad \Psi_2(\mathbf{r}) = (-1)^k \gamma G_l^k \cdot \frac{\partial^{l-k}}{\partial h^{l-k}} \left\{ \left(\frac{a}{h}\right)^{2k+1} \frac{\lambda}{r_K} \int_0^{r_K} \frac{(r_K/x)^{1-\lambda-k}}{r_x^{k+1}} Y_k^k(\theta_x, \varphi_x) dx \right\} .$$

We note that $\Psi_1$ is almost identical to the image potential of the multipole source outside a conducting sphere, except for the factor $\gamma$. Applying the result of [24], we obtain

$$(43) \qquad\qquad \Psi_1(\mathbf{r}) = \sum_{j=k}^{l} \frac{N_{lj}^k}{r_g^{j+1}} Y_j^k(\theta_g, \varphi_g) .$$

We now analyze $\Psi_2$. We first rewrite $\Psi_2$,

$$(44) \qquad\qquad \Psi_2(\mathbf{r}) = G_l^k \cdot \frac{\partial^{l-k}}{\partial h^{l-k}} \left\{ u(h) f(g(h)) \right\} ,$$

where

$$(45) \qquad\qquad u(h) = (-1)^k \gamma \left(\frac{a}{h}\right)^{2k+1} \frac{\lambda}{r_K}$$

and

$$(46) \qquad\qquad f(g(h)) = \int_0^{g(h)} \left[\frac{g(h)}{x}\right]^{1-\lambda-k} \frac{1}{r_x^{k+1}} Y_k^k(\theta_x, \varphi_x) dx$$

with

$$(47) \qquad\qquad g(h) = r_K = \frac{a^2}{h} .$$

Applying the Leibniz rule to (44) leads to

$$(48) \qquad\qquad \Psi_2(\mathbf{r}) = G_l^k \sum_{i=0}^{l-k} \binom{l-k}{i} f^{(i)}(g(h)) u^{(l-k-i)}(h) .$$

Applying Faà di Bruno's formula (Lemma 9) to $f^{(i)}(g(h))$, we have

$$(49) \quad \begin{aligned} \Psi_2(\mathbf{r}) = G_l^k \sum_{i=0}^{l-k} \sum_{m=1}^{i} \binom{l-k}{i} & u^{(l-k-i)}(h) f^{(m)}(g) B_{i,m}[g', g'', \ldots, g^{(i-m+1)}] \\ &+ G_l^k u^{(l-k-i)}(h) f(g(h)) . \end{aligned}$$

It is straightforward to compute $u^{(l-k-i)}(h)$,

$$(50) \qquad\qquad u(h)^{(l-k-i)} = (-1)^{l-i} \gamma \lambda \frac{(2k)!}{(k+l-i)!} \frac{a^{2k-1}}{h^{k+l-i}} .$$

$f^{(m)}(g)$ can be computed similarly, although the procedure is much more lengthy. Substituting the expression for $f^{(m)}(g)$ and (50) into (49) and simplifying the resulting expression, we find that

$$(51) \qquad\qquad \Psi_2(\mathbf{r}) = -\sum_{j=k}^{l} \frac{\lambda N_{lj}^k}{r_K} \int_0^{r_K} \frac{(r_K/x)^{1-\lambda-j}}{r_x^{j+1}} Y_j^k(\theta_x, \varphi_x) dx ,$$

where the coefficients $N_{lj}^k$ are given in (38). Substitution of (43) and (51) into (40) yields (36). The induced potential (37) inside the sphere can be obtained in a similar manner.                                                                          □

*Remark* 11. When $l = k$, (36) and (37) reduce to the image potentials for a sectoral multipole, (15) and (16). When $l = 1$, $k = 0$, (36) and (37) reproduce the classic result for the image potentials of a dipole source outside a dielectric sphere [31].

*Remark* 12. We could alternatively use the following recurrence relations to calculate the coefficients $N_{lj}^k$:

$$(52) \quad \begin{cases} N_{lk}^k = (-1)^{l+1}\gamma\sqrt{\left(\begin{array}{c} l+k \\ l-k \end{array}\right)}\dfrac{a^{2k+1}}{h^{l+k+1}}G_l^k \,, \\[2em] N_{lj}^k = (-1)^{l+1}\gamma\sqrt{\left(\begin{array}{c} l+j \\ l+k \end{array}\right)\left(\begin{array}{c} l+j \\ l-k \end{array}\right)}\dfrac{a^{2j+1}}{h^{l+j+1}}G_l^k \\[1em] \quad - \displaystyle\sum_{i=1}^{j-k} N_{j-i}^k \sqrt{\left(\begin{array}{c} j+k \\ i \end{array}\right)\left(\begin{array}{c} j-k \\ i \end{array}\right)}\left(\dfrac{a^2}{h}\right)^i \,, \quad j = k+1,\dots,l \,. \end{cases}$$

However, this does not improve the speed in numerical simulations, where all combinatorial factors are precomputed and tabulated.

*Remark* 13. Equations (36)–(37) contain singular integrals with a $x^{\lambda-1}$ singularity at the origin (for the integral in (37), the change of variables $h/x = t$ should be made first). We apply the Gauss–Jacobi quadrature to discretize these integrals. In practice, 2–5 quadrature points (depending on the distance of the source point to the sphere) suffice to obtain 6-digit accuracy.

*Remark* 14. We have only presented the case in which the multipole source is located on the $+z$-axis. For a general source location $\mathbf{c} = (x_c, y_c, z_c)$ outside the sphere, the following procedure is applied to find the image potentials. First, the coordinate system is rotated so that the multipole source is located at $(0, 0, |\mathbf{c}|)$; second, the corresponding rotation matrices are applied to the multipole expansion coefficients [40, pp. 275–277]; third, the generalized image formula in Theorem 10 is used to obtain the image multipole coefficients for the rotated multipole source; and finally, the image multipole coefficients are rotated back to the original coordinate system.

**4. Numerical algorithms.** We present the hybrid numerical scheme for systems of dielectric spheres and ions (Figure 1). We denote the total number of spheres by $M$, the total number of point charges by $N$, and the order of the spherical harmonic expansion by $p$.

**4.1. Case I: Well-separated spheres and ions.** Here we present the procedure of the MoM for solving (2)–(4). This method is efficient when all dielectric spheres and point charges are well separated.

The potential in the exterior region can be written as a sum of two parts,

$$(53) \qquad\qquad \Phi(\mathbf{r}) = \Phi_0(\mathbf{r}) + \Psi(\mathbf{r}) \,, \quad \mathbf{r} \in \Omega^c \,,$$

where $\Phi_0(\mathbf{r})$ is the direct Coulomb contribution due to the point sources,

$$(54) \qquad\qquad \Phi_0(\mathbf{r}) = \sum_{i=1}^{N} \frac{q_i}{4\pi\epsilon_s|\mathbf{r} - \mathbf{r}_i|} \,,$$

and $\Psi(\mathbf{r})$ is the induced potential due to the presence of dielectric spheres. It is a harmonic function and can be represented in terms of (truncated) multipole expansions,

$$(55) \qquad \Psi(\mathbf{r}) = \sum_{j=1}^{M} \sum_{m,n}^{p} \frac{B_{nm}^{j}}{r_{j}^{n+1}} Y_{n}^{m}(\theta_{j}, \varphi_{j}) \,,$$

where $(r_j, \theta_j, \varphi_j)$ are the spherical coordinates of $\mathbf{r} - \mathbf{o}_j$ for $j = 1, 2, \ldots, M$, respectively. Similarly, the electrostatic potential inside each sphere can be represented by a (truncated) local expansion,

$$(56) \qquad \Phi(\mathbf{r}) = \sum_{m,n}^{p} A_{nm}^{j} r_{j}^{n} Y_{n}^{m}(\theta_{j}, \varphi_{j}) \,, \quad \mathbf{r} \in S_{j} \text{ for } j = 1, \ldots, M \,.$$

Equations (53)–(56) represent a general solution of the studied problem with the moments of the expansions, $A_{nm}^{j}$ and $B_{nm}^{j}$, to be determined.

For the $k$th sphere, we first represent $\Phi_0$ in terms of the local expansion,

$$(57) \qquad \Phi_0(\mathbf{r}) = \sum_{m,n}^{p} C_{nm}^{k} r_{k}^{n} Y_{n}^{m}(\theta_{k}, \varphi_{k})$$

with

$$(58) \qquad C_{nm}^{k} = \sum_{i=1}^{N} \frac{q_i}{4\pi\epsilon_s} \frac{Y_n^{-m}(\alpha_{ik}, \beta_{ik})}{\rho_{ik}^{n+1}} \,.$$

To simplify our notation, we denote $A^k = \{A_{nm}^k,\ n = 0, \ldots, p; m = -n, \ldots, n\}$, and similarly for $B^k$ and $C^k$. Substituting the expansions (55)–(57) into the boundary conditions (3)–(4), we obtain

$$(59) \qquad C_{nm}^{k} + \frac{B_{nm}^{k}}{a_{k}^{2n+1}} + \sum_{\substack{j=1 \\ j \neq k}}^{M} \left( \mathcal{T}_{M2L}^{kj} B^{j} \right)_{nm} = A_{nm}^{k} \,,$$

$$(60) \qquad C_{nm}^{k} - \frac{(n+1)}{n} \frac{B_{nm}^{k}}{a_{k}^{2n+1}} + \sum_{\substack{j=1 \\ j \neq k}}^{M} \left( \mathcal{T}_{M2L}^{kj} B^{j} \right)_{nm} = \frac{\epsilon_k}{\epsilon_s} A_{nm}^{k}$$

for $n = 0, \ldots, p;\ m = -n, \ldots, n;\ k = 1, \ldots, M$. Here $\mathcal{T}_{M2L}^{kj}$ denotes the standard multipole-to-local (M2L) translation operator which translates the multipole expansion at the $j$th sphere to the local expansion at the $k$th sphere [10, 35].

When $p$ is small, the linear system (59)–(60) is well-conditioned and may be solved efficiently using iterative solvers such as GMRES.

*Remark* 15. For some applications, one is interested in the exterior potential only. Eliminating $A^k$ from (59)–(60) leads to a linear system for $B^k$,

$$(61) \qquad \frac{(n+1)\epsilon_s + n\epsilon_k}{n(\epsilon_s - \epsilon_k)} \frac{B_{nm}^{k}}{a_{k}^{2n+1}} - \sum_{\substack{j=1 \\ j \neq k}}^{M} \left( \mathcal{T}_{M2L}^{kj} B^{j} \right)_{nm} = C_{nm}^{k} \,, \quad k = 1, \ldots, M \,.$$

This will halve the size of the linear system.

*Remark* 16. The calculation of the coefficients $C_{nm}^k$ is carried out as follows. First, compute $\Phi_0$ at $Mp^2$ grid points (i.e., $p^2$ points for each sphere) using the FMM; this step requires $\mathcal{O}(N + Mp^2)$ operations. Second, use the spherical harmonic transform to evaluate $C_{nm}^k$ for each $k$; this step costs $\mathcal{O}(Mp^3)$ operations.

*Remark* 17. Since all $M$ spheres interact, the system matrix is dense and the matrix–vector product in each iteration takes $\mathcal{O}(M^2p^3)$ operations if the naive direct method is used. However, one can easily modify the FMM to reduce the cost to $\mathcal{O}(Mp^3)$, i.e., linear complexity with respect to the total number of dielectric spheres. See, e.g., [41, 42] for details.

**4.2. Case II: Some ions close to dielectric spheres.** The order $p$ of the spherical harmonic expansion will increase sharply if some ions are very close to a sphere. In this case, we use the method of image charges to take into account the effect of nearby charges. Specifically, we modify the potential inside the $k$th sphere,

$$(62) \qquad \Phi(\mathbf{r}) = \sum_{m,n}^p A_{nm}^k r_k^n Y_n^m(\theta_k, \varphi_k) + \Phi_{0k}^{(\mathrm{in})}(\mathbf{r}) , \quad \mathbf{r} \in S_k ,$$

and the potential in the exterior region,

$$(63) \qquad \Phi(\mathbf{r}) = \Phi_0(\mathbf{r}) + \sum_{k=1}^M \sum_{m,n}^p \frac{B_{nm}^k}{r_k^{n+1}} Y_n^m(\theta_k, \varphi_k) + \sum_{k=1}^M \Phi_{0k}^{(\mathrm{ex})}(\mathbf{r}) , \quad \mathbf{r} \in \Omega^c ,$$

where $\Phi_{0k}^{(\mathrm{in})}$ and $\Phi_{0k}^{(\mathrm{ex})}$ are the image potentials inside and outside $S_k$ due to the point charges that are close to $S_k$. The remaining procedure is then identical to that of the MoM (section 4.1).

*Remark* 18. We consider a point charge *close* to a sphere if the distance of the charge to the sphere surface is less than $\eta(\varepsilon)a$. Here $\eta(\varepsilon)$ is a parameter depending on the accuracy $\varepsilon$ required by the application. For 6-digit accuracy, we choose $\eta = 5$; for 2-digit accuracy, $\eta = 1$ should be sufficient for most practical applications.

*Remark* 19. We only add the contribution of the image charges to the system when point charges are close to a sphere. Therefore, the total number of charges in the system is $\mathcal{O}(N + M)$ for most practical applications and hence does not change the complexity of the algorithm.

*Remark* 20. Similar to the discretization of line image multipoles, we discretize the line image charges in (11) using the Gauss–Jacobi quadrature. The infinite integral in (11) can also be treated similarly to that of image multipoles, as stated in Remark 13.

**4.3. Case III: Dielectric spheres close to each other.** If dielectric spheres are close to each other, we use the image potential of multipoles to reduce the ill-conditioning of the linear system. Assume that the $j$th sphere is close to the $k$th sphere. Then the multipole expansion outside the $k$th sphere has coefficients

$$(64) \qquad\qquad B^k + \mathcal{R}_{kj}^{(\mathrm{ex})} B^j ,$$

and the local expansion inside the $k$th sphere has coefficients

$$(65) \qquad\qquad A^k + \mathcal{R}_{kj}^{(\mathrm{in})} B^j ,$$

where $\mathcal{R}_{kj}^{(\text{ex})} B^j$ are the multipole expansion coefficients of the image potential outside the $k$th sphere due to the multipole source $B^j$ on the $j$th sphere, and $\mathcal{R}_{kj}^{(\text{in})} B^j$ are the local expansion coefficients of the image potential inside the $k$th sphere due to the same multipole source. Likewise, we need to add the contribution of the image multipoles to the $j$th sphere as well. All these coefficients can be computed using Theorem 10 and Remark 14.

For the general case, we define $c_k^s$ as the set of indices of the spheres that are close to the $k$th sphere. That is,

$$(66) \qquad c_k^s = \{l \mid |\mathbf{o}_l - \mathbf{o}_k| - (a_l + a_k) < \eta_{\text{sph}}, \quad l \in \{1, \dots, M\}\},$$

where $\eta_{\text{sph}}$ is the surface-to-surface distance parameter for pairs of close spheres. This changes (64)–(65) as follows:

$$(67) \qquad B^k + \sum_{j \in c_k^s} \mathcal{R}_{kj}^{\text{ex}} B^j,$$

$$(68) \qquad A^k + \sum_{j \in c_k^s} \mathcal{R}_{kj}^{\text{in}} B^j.$$

We then use the boundary conditions to set up a linear system for the coefficients $A^k$ and $B^k$ $(k = 1, \dots, M)$.

*Remark* 21. In the case of symmetric unit spheres, generally $\eta_{\text{sph}} = 4$ can reach 6-digit accuracy. For 2-digit accuracy, $\eta_{\text{sph}} = 1$ should be sufficient.

*Remark* 22. It is clear that when the image potentials of point charges are added, the only change in the matrix is a reduction of the order $p$ of the spherical harmonic expansion. However, when the image potentials of multipoles are added, the system matrix changes dramatically even if $p$ is kept the same. This is exactly what one would like to achieve, since the original matrix would be ill-conditioned for the cases where some spheres are close to each other.

**4.4. The hybrid method.** We are now in a position to describe the hybrid method for solving the Poisson equation in a composite consisting of a collection of arbitrarily spaced dielectric spheres and ions. It combines the MoM with the classical image-charge method (CICM) for *close* point–interface interactions and the GICM for *close* interface–interface interactions, and it uses the FMM to speed up the computation of particle–particle and sphere–sphere interactions. The resulting linear system is well-conditioned for most practical applications, and the overall algorithm achieves optimal complexity.

*Remark* 23. We use the publicly available software package FMM3DLIB [43] for the harmonic FMM. This package is reasonably fast but not highly optimized. It assumes, for example, that all charge strengths are complex, and uses "point-and-shoot" translation operators instead of diagonal translation operators [10].

We now summarize the hybrid method in Algorithm 1.

---

**Algorithm 1.** Hybrid method for systems of dielectric spheres and ions.

---

**Require:** Given a spherical harmonic expansion order $p$, dielectric constant $\epsilon_s$ for the medium, sphere radius $a_i$, sphere centers $\mathbf{o}_i$ and dielectric constant $\epsilon_i$ ($i = 1, \ldots, M$), ion locations $\mathbf{r}_j$ and charges $q_j$ ($j = 1, \ldots, N$), compute the induced Coulomb potential.

1: Construct a set of quadrature nodes and weights on each sphere (Gauss–Legendre nodes along the $\theta$ direction, and equispaced points along the $\varphi$ direction, with $2p$ points in each direction) to be used for the spherical harmonic transform.

2: With all sphere centers and ion locations as input, build an adaptive oct-tree. For each sphere $k$, find the set of spheres $c_k^s$ and the set of point charges $c_k^p$ that are *close* to it. For most applications, both $c_k^s$ and $c_k^p$ are $\mathcal{O}(1)$.

3: Use the FMM to evaluate, on all spherical grids, the potentials generated in the exterior region by all point charges and their images inside the spheres. This step requires $\mathcal{O}(N + Mp^2)$ operations. Evaluate on each spherical grid the potential generated inside this sphere by the image charges outside it. This step costs at most $\mathcal{O}(Mp^2)$ for most applications, since each $c_k^p$ is $\mathcal{O}(1)$.

4: Apply a spherical harmonic transform to obtain the multipole and local expansion coefficients due to point charges and possibly their image charges. This step produces the right-hand side of the linear system and requires $\mathcal{O}(Mp^3)$ operations.

5: Use an iterative solver such as GMRES to solve the linear system and obtain the local and multipole coefficients $A^k$ and $B^k$. The sphere–sphere interactions, which involve the M2L translation operators, are accelerated by the FMM and have $\mathcal{O}(Mp^3)$ complexity. The action on the multipole coefficient $B^k$ due to the presence of image multipoles is computed via Theorem 10 and Remark 14 and has at most $\mathcal{O}(Mp^3)$ complexity as well.

6: Use the FMM again to evaluate the potential or the field at the desired target locations. This step has $\mathcal{O}(N + Mp^2 + N_T)$ complexity, with $N_T$ the number of target points.

---

**5. Numerical examples.** In this section, we present numerical results to demonstrate the well-conditioning, accuracy, and timing performance of Algorithm 1. We have implemented our algorithm in C with OpenMP to parallelize some `for` loops. In all the numerical tests, the required precision for GMRES is set to $10^{-9}$ and the precision for the FMM is set to $10^{-9}$ as well. All spheres are of the same size with radius $a$ rescaled to 1. The dielectric constant outside the spheres is taken to be 80 to represent the water solvent and inside the spheres is equal to 2 (to represent, e.g., hydrocarbon nanoparticles). We set the *closeness* parameter $\eta_{\mathrm{sph}}$ to 4 for sphere–sphere interactions. We calculate the total potential energy of the system to verify the accuracy. The total energy is defined as

$$(69) \qquad E_{\mathrm{total}} = \sum_{i=1}^{N} \frac{q_i}{2} \Phi(\mathbf{r}_i),$$

and the potential is expressed as

$$(70) \qquad \Phi(\mathbf{r}) = \Phi_0(\mathbf{r}) + \sum_{k=1}^{M} \Phi_{0k}^{(\text{ex})}(\mathbf{r}) + \sum_{k=1}^{M} \sum_{m,n}^{p} \left( B_{nm}^k + \sum_{j \in c_k^s} \mathcal{R}_{kj}^{\text{ex}} B^j \right) \frac{Y_n^m(\theta_k, \varphi_k)}{r_k^{n+1}},$$

where the second term comes from ions close to surfaces, and the second term in the bracket is due to the close-sphere pairs. For all tests, the reference solutions are obtained via a self-consistent check with 10-digit precision (in some cases also cross-checked against the results of the simple MoM), and the relative errors are then computed to show the accuracy. The timing results are obtained on a 64-core machine (4 AMD Opteron Processors Model 6272 2.1 GHz with 16 cores each), where the number of threads is set to 60. For the first three examples, we study the effectiveness of the hybrid method in reducing the order $p$ of the spherical harmonic expansion and the number of iterations for GMRES when point charges are close to spheres or spheres are close to each other. For cases involving random arrangements of charges (Examples 2–5), we average over four random configurations.

In the following tables, the first column lists the smallest distance between a point and a sphere or between two spheres. We separately list the performance of the MoM and the hybrid method, where $p$ is the order of the spherical harmonic expansion, #iter is the number of iterations needed by GMRES, and the last column lists the error in the total electrostatic energy of the systems. For the hybrid method, the minimal spherical harmonic expansion order to achieve 6-digit accuracy $p = p_{\min}$ is listed.

**Example 1: Source charge approaching an interface.** We consider a positive unit source charge that approaches one of the interfaces in a system of two neutral, well-separated unit dielectric spheres. The spheres are centered at $(\pm 6, 0, 0)$. A unit point charge is placed at $\mathbf{r}_s = (5 - \Delta, 0, 0)$ with $\Delta > 0$; that is, the distance between the point charge and the right-hand sphere is $\Delta$. We vary $\Delta$ from 5 to $10^{-6}$ and compare the conventional MoM and our scheme, which in this case is the MoM/CICM method. We list the order to achieve 6-digit accuracy in Table 1, and also the number of GMRES iterations required for both methods as a comparison. If the MoM does not reach the accuracy requirement after $p = 350$, we omit the number of iterations and the accuracy, since for $p = 350$ there are $8p^2 \approx 10^6$ unknowns (with $A_{nm}^k$ eliminated from the system and solving for $B_{nm}^k$ (61) only, per Remark 15) and the simple MoM becomes very inefficient.

Table 1 indicates that, as the source charge approaches the interface, the hybrid method can reach an accuracy of six digits with $p = 4$ even when the distance $\Delta$ is as small as $10^{-6}$. For the MoM, to reach the accuracy, the order increases rapidly with decreasing $\Delta$, and it becomes greater than 350 when $\Delta \leq 0.01$. Moreover, the hybrid method takes at most six GMRES iterations to reach convergence for the entire range of charge–surface separations examined, whereas for the MoM the number of GMRES iterations grows with decreasing $\Delta$.

**Example 2: Two spheres approaching each other.** In this example, we randomly place 100 positive monovalent ions around two neutral dielectric spheres of unit radius within a cube of edge length 20 and vary the surface separation $\delta$ between the spheres from 10 to $10^{-6}$. We calculate the potential energy via the conventional MoM and via the MoM/GICM hybrid method to 6-digit accuracy. In the MoM, the order $p$ of the spherical harmonic expansion increases rapidly as the two spheres approach each other; see Table 2. By contrast, for the hybrid method, $p$ is maintained at 6 and the number of GMRES iterations increases only moderately even

Table 1

*Accuracy and convergence of the MoM and the hybrid method for the case where a source charge is approaching one of two spherical interfaces. We vary the source–interface nearest distance $\Delta$ while retaining at least 6-digit accuracy in the electrostatic energy for both methods.*

| | Method of moments | | | Hybrid method | | |
|---|---|---|---|---|---|---|
| $\Delta$ | $p$ | # iter | Error | $p_{\min}$ | # iter | Error |
| 5 | 6 | 6 | 1.3E-9 | 4 | 4 | 6.1E-10 |
| 2 | 10 | 9 | 4.0E-8 | 4 | 6 | 1.9E-9 |
| 1 | 15 | 10 | 7.9E-8 | 4 | 6 | 3.2E-9 |
| 0.5 | 25 | 11 | 1.4E-7 | 4 | 6 | 5.6E-8 |
| 0.2 | 45 | 12 | 1.3E-7 | 4 | 6 | 8.8E-8 |
| 0.1 | 70 | 12 | 2.9E-6 | 4 | 6 | 9.4E-8 |
| 1.0E−2 | > 350 | - | - | 4 | 6 | 1.2E-7 |
| 1.0E−3 | > 350 | - | - | 4 | 6 | 2.7E-7 |
| 1.0E−4 | > 350 | - | - | 4 | 6 | 3.2E-7 |
| 1.0E−5 | > 350 | - | - | 4 | 6 | 4.9E-7 |
| 1.0E−6 | > 350 | - | - | 4 | 6 | 7.6E-7 |

Table 2

*Accuracy and convergence of the hybrid method for the case when two spheres are approaching each other, with 100 source charges surrounding them. $\delta$ is the distance between the two spheres.*

| | Method of moments | | | Hybrid method | | |
|---|---|---|---|---|---|---|
| $\delta$ | $p$ | # iter | Error | $p_{\min}$ | # iter | Error |
| 10 | 120 | 12 | 2.0E-6 | 6 | 5 | 4.9E-8 |
| 5 | 180 | 13 | 3.5E-7 | 6 | 7 | 6.0E-8 |
| 2 | 300 | 14 | 3.7E-7 | 6 | 8 | 9.8E-8 |
| 1 | >350 | - | - | 6 | 9 | 1.3E-7 |
| 0.5 | >350 | - | - | 6 | 9 | 2.6E-7 |
| 0.2 | >350 | - | - | 6 | 10 | 3.3E-7 |
| 0.1 | >350 | - | - | 6 | 11 | 4.3E-7 |
| 1.0E-2 | >350 | - | - | 6 | 11 | 7.6E-7 |
| 1.0E-3 | >350 | - | - | 6 | 12 | 7.8E-7 |
| 1.0E-4 | >350 | - | - | 6 | 12 | 7.7E-7 |
| 1.0E-5 | >350 | - | - | 6 | 12 | 8.1E-7 |
| 1.0E-6 | >350 | - | - | 6 | 12 | 8.0E-7 |

when the spheres are as close as $10^{-6}$. This illustrates how the hybrid method is able to very effectively reduce the ill-conditioning of the system due to close-to-touching geometries.

**Example 3: Three spheres approaching each other.** We now consider an even more challenging case. We place 100 positive monovalent ions around three neutral unit spheres that are located on the vertices of an equilateral triangle and let the spheres approach each other simultaneously. The spheres and ions are contained within a cube of edge length 20. The distance between each pair of spheres ranges from 10 to $10^{-6}$. This is an even more stringent test for the hybrid method, since at first sight it may seem that the image potentials of the multipole expansions can only ameliorate the ill-conditioning of the interaction between *two* close spheres.

Table 3 lists the numerical results for both the MoM and the hybrid method. For the MoM, the order $p$ of the spherical harmonic expansion increases again with decreasing separation, but now even more sharply than in Table 2. Meanwhile, for the hybrid method, $p$ remains equal to 8 even when all three spheres are nearly touching. The number of GMRES iterations is less than 20 even in the worst case. This example clearly demonstrates that our hybrid method can reduce the ill-conditioning of the

TABLE 3

*Accuracy and convergence of the hybrid method for the case of three spheres placed on the vertices of an equilateral triangle, with 100 source charges surrounding them. $\delta$ is the distance between each pair of spheres.*

| | Method of moments | | | Hybrid method | | |
|---|---|---|---|---|---|---|
| $\delta$ | $p$ | # iter | Error | $p_{\min}$ | # iter | Error |
| 10 | 170 | 14 | 2.0E-7 | 8 | 6 | 2.9E-8 |
| 5 | 340 | 16 | 6.9E-7 | 8 | 7 | 5.0E-8 |
| 2 | $> 350$ | - | - | 8 | 9 | 9.3E-8 |
| 1 | $> 350$ | - | - | 8 | 10 | 2.5E-7 |
| 0.5 | $> 350$ | - | - | 8 | 11 | 3.3E-7 |
| 0.2 | $> 350$ | - | - | 8 | 13 | 2.9E-7 |
| 0.1 | $> 350$ | - | - | 8 | 14 | 3.9E-7 |
| 1.0E-2 | $> 350$ | - | - | 8 | 17 | 8.1E-7 |
| 1.0E-3 | $> 350$ | - | - | 8 | 19 | 8.9E-7 |
| 1.0E-4 | $> 350$ | - | - | 8 | 18 | 9.1E-7 |
| 1.0E-5 | $> 350$ | - | - | 8 | 19 | 8.8E-7 |
| 1.0E-6 | $> 350$ | - | - | 8 | 18 | 8.8E-7 |

system very effectively even when more than two spheres are close to each other.

**Example 4: Timing results for many point charges.** To demonstrate the efficiency of the FMM in the hybrid method, we consider the following system. We place eight unit spheres on a cube and $N$ point charges around them. The spheres are centered at the vertices of a cube of size $2 + 10^{-6}$; i.e., the smallest surface separation between two spheres is only $10^{-6}$. We vary the number of point charges $N$ from $10^3$ to $10^7$. Figure 2 shows the total time (in seconds) required to compute the electrostatic energy. In combination with the FMM, the hybrid method displays linear scaling. For a system of 10 million particles, the FMM yields an acceleration by four orders of magnitude compared to direct summation, reducing the calculation from $6 \times 10^5$ seconds to 50 seconds.

**Example 5: Timing results for many dielectric spheres.** To demonstrate that the hybrid method, when combined with the FMM, scales well not only with the number of point charges but also with the number of dielectric spheres, we randomly place $M$ dielectric unit spheres ($M$ ranging from 2 to $10^4$) in a cubic box. The box size is adapted for different $M$ so that the volume fraction of the dielectric spheres is kept constant at 20%. In addition, we randomly place $N = 1000$ point charges around the dielectric interfaces. Figure 3 shows the total computing time as a function of $M$, which again agrees well with linear scaling. For 10000 dielectric spheres, the hybrid method with the FMM is able to compute the total electrostatic energy in approximately 220 seconds, compared to $5 \times 10^3$ seconds for the hybrid method combined with direct summation.

**6. Summary and conclusions.** In conclusion, we have analytically generalized the method of images for point charges near dielectric spheres to arbitrary multipole expansions. We then combined this method of image multipoles with the MoM and the method of image charges to construct a hybrid method for the solution of the Poisson equation for systems consisting of *closely spaced* dielectric spheres and ions. Our method removes the ill-conditioning of such systems due to close charge–surface
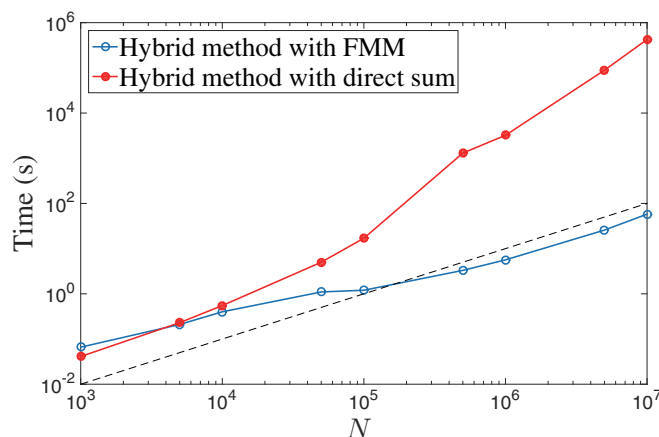
Fig. 2. *Total computing time for the evaluation of the potential energy of $N$ point charges near eight dielectric unit spheres placed on the vertices of a cube. The cube has side length $2 + 10^{-6}$; i.e., the surface separation between two neighboring spheres is $10^{-6}$. The accuracy is set to $10^{-6}$. In conjunction with the FMM, the hybrid method (blue open symbols) displays linear scaling (dashed line) with the number of particles, greatly accelerating the calculation compared with direct summation (red closed symbols).*
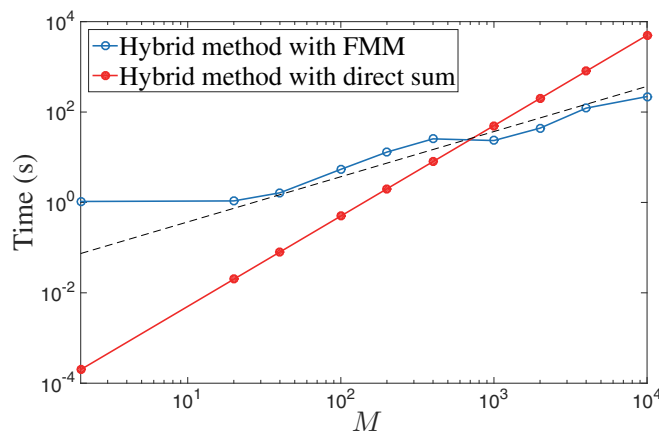


Fig. 3. *Total computing time for the electrostatic energy of a single configuration as a function of the number of dielectric spheres $M$. These spheres are randomly placed inside a cubic box, at a fixed volume fraction of $20\%$. In addition, $1000$ point charges are generated, randomly surrounding the spheres. The required accuracy is set to $10^{-6}$. When combined with the FMM, the hybrid method displays linear scaling behavior.*

and interface–interface interactions. Through combining this method with the FMM to speed up the ion–ion and sphere–sphere interactions we achieve $\mathcal{O}(N + M)$ (i.e., optimal) complexity for systems with $N$ ions and $M$ dielectric spheres.

When the particles are not of spherical shape, we anticipate that a boundary integral formulation will be possible that—when combined with the FMM, the recently developed QBX method, and adaptive mesh refinement—will be capable of efficiently and accurately solving systems of large numbers of arbitrarily shaped dielectric objects

and charged particles.

In addition, we are currently applying the hybrid method proposed here in large-scale studies of the role of dielectric effects in nanoparticle self-assembly.

## REFERENCES

[1] R. H. FRENCH, V. A. PARSEGIAN, R. PODGORNIK, R. F. RAJTER, A. JAGOTA, J. LUO, D. ASTHAGIRI, M. K. CHAUDHURY, Y.-M. CHIANG, S. GRANICK, S. KALININ, M. KARDAR, R. KJELLANDER, D. C. LANGRETH, J. LEWIS, S. LUSTIG, D. WESOLOWSKI, J. S. WETTLAUFER, W.-Y. CHING, M. FINNIS, F. HOULIHAN, O. A. VON LILIENFELD, C. J. VAN OSS, AND T. ZEMB, *Long range interactions in nanoscale science*, Rev. Modern Phys., 82 (2010), pp. 1887–1944, http://dx.doi.org/10.1103/RevModPhys.82.1887.

[2] D. A. WALKER, B. KOWALCZYK, M. OLVERA DE LA CRUZ, AND B. A. GRZYBOWSKI, *Electrostatics at the nanoscale*, Nanoscale, 3 (2011), pp. 1316–1344, http://dx.doi.org/10.1039/C0NR00698J.

[3] J. LIU AND E. LUIJTEN, *Stabilization of colloidal suspensions by means of highly charged nanoparticles*, Phys. Rev. Lett., 93 (2004), 247802, http://dx.doi.org/10.1103/PhysRevLett.93.247802.

[4] K. BARROS AND E. LUIJTEN, *Dielectric effects in the self-assembly of binary colloidal aggregates*, Phys. Rev. Lett., 113 (2014), 017801, http://dx.doi.org/10.1103/PhysRevLett.113.017801.

[5] J. REŠČIČS AND P. LINSE, *Potential of mean force between charged colloids: Effect of dielectric discontinuities*, J. Chem. Phys., 129 (2008), 114505, http://dx.doi.org/10.1063/1.2971038.

[6] J. D. JACKSON, *Classical Electrodynamics*, 3rd ed., Wiley, New York, 1999.

[7] H. HOSHI, M. SAKURAI, Y. INOUE, AND R. CHÛJÔ, *Medium effects on the molecular electronic structure. I. The formulation of a theory for the estimation of a molecular electronic structure surrounded by an anisotropic medium*, J. Chem. Phys., 87 (1987), pp. 1107–1115, http://dx.doi.org/10.1063/1.453343.

[8] R. BHARADWAJ, A. WINDEMUTH, S. SRIDHARAN, B. HONIG, AND A. NICHOLLS, *The fast multipole boundary element method for molecular electrostatics: An optimal approach for large systems*, J. Comput. Chem., 16 (1995), pp. 898–913, http://dx.doi.org/10.1002/jcc.540160707.

[9] K. BARROS, D. SINKOVITS, AND E. LUIJTEN, *Efficient and accurate simulation of dynamic dielectric objects*, J. Chem. Phys., 140 (2014), 064903, http://dx.doi.org/10.1063/1.4863451.

[10] H. CHENG, L. GREENGARD, AND V. ROKHLIN, *A fast adaptive multipole algorithm in three dimensions*, J. Comput. Phys., 155 (1999), pp. 468–498, http://dx.doi.org/10.1006/jcph.1999.6355.

[11] L. GREENGARD AND V. ROKHLIN, *A fast algorithm for particle simulations*, J. Comput. Phys., 73 (1987), pp. 325–348.

[12] L. YING, G. BIROS, AND D. ZORIN, *A kernel-independent adaptive fast multipole algorithm in two and three dimensions*, J. Comput. Phys., 196 (2004), pp. 591–626, http://dx.doi.org/10.1016/j.jcp.2003.11.021.

[13] D. R. MCKENZIE, R. C. MCPHEDRAN, AND G. H. DERRICK, *The conductivity of lattices of spheres. II. The body centred and face centred cubic lattices*, P. Roy. Soc. A-Math. Phy., 362 (1978), pp. 211–232, http://dx.doi.org/10.1098/rspa.1978.0129.

[14] R. C. MCPHEDRAN AND D. R. MCKENZIE, *The conductivity of lattices of spheres. I. The simple cubic lattice*, P. Roy. Soc. A-Math. Phy., 359 (1978), pp. 45–63, http://dx.doi.org/10.1098/rspa.1978.0031.

[15] A. S. SANGANI AND A. ACRIVOS, *The effective conductivity of a periodic array of spheres*, P. Roy. Soc. A-Math. Phy., 386 (1983), pp. 263–275, http://dx.doi.org/10.1098/rspa.1983.0036.

[16] K. HINSEN AND B. FELDERHOF, *Dielectric constant of a suspension of uniform spheres*, Phys. Rev. B, 46 (1992), pp. 12955–12963, http://dx.doi.org/10.1103/PhysRevB.46.12955.

[17] L. GREENGARD AND M. MOURA, *On the numerical evaluation of electrostatic fields in composite materials*, Acta Numer., 3 (1994), pp. 379–410, http://dx.doi.org/10.1017/S0962492900002464.

[18] Y. SAAD AND M. H. SCHULTZ, *GMRES: A generalized minimal residual algorithm for solving nonsymmetric linear systems*, SIAM J. Sci. Comput., 7 (1986), pp. 856–869, http://dx.doi.org/10.1137/0907058.

[19] M. G. DUFFY, *Quadrature over a pyramid or cube of integrands with a singularity at a vertex*, SIAM J. Numer. Anal., 19 (1982), pp. 1260–1262, http://dx.doi.org/10.1137/0719090.

[20] Z. GIMBUTAS AND S. VEERAPANENI, *A fast algorithm for spherical grid rotations and its appli-*

cation to singular quadrature, SIAM J. Sci. Comput., 35 (2013), pp. A2738–A2751, http://dx.doi.org/10.1137/120900587.

[21] A. KLOECKNER, A. BARNETT, L. GREENGARD, AND M. O'NEIL, Quadrature by expansion: A new method for the evaluation of layer potentials, J. Comput. Phys., 252 (2013), pp. 332–349, http://dx.doi.org/10.1016/j.jcp.2013.06.027.

[22] C. L. EPSTEIN, L. GREENGARD, AND A. KLÖCKNER, On the convergence of local expansions of layer potentials, SIAM J. Numer. Anal., 51 (2013), pp. 2660–2679, http://dx.doi.org/10.1137/120902859.

[23] M. RACHH, Integral Equation Methods for Problems in Electrostatics, Elastostatics and Viscous Flow, Ph.D. thesis, New York University, New York, NY, 2015.

[24] H. CHENG, On the method of images for systems of closely spaced conducting spheres, SIAM J. Appl. Math., 61 (2000), pp. 1324–1337, http://dx.doi.org/10.1137/S0036139999364992.

[25] W. YING AND J. BEALE, A fast accurate boundary integral method for potentials on closely packed cells, Commun. Comput. Phys., 14 (2013), pp. 1073–1093, http://dx.doi.org/10.4208/cicp.210612.240113a.

[26] W. THOMSON (LORD KELVIN), Extrait d'une lettre de M. William Thomson (reported by A. M. Liouville), J. Math. Pure Appl, 10 (1845), pp. 364–367.

[27] C. NEUMANN, Hydrodynamische Untersuchungen, nebst einem Anhange über die Probleme der Elektrostatik und der magnetischen Induction, B.G. Teubner, Leipzig, 1883.

[28] F. OLYSLAGER AND I. V. LINDELL, Closed form solutions of Maxwell's equations in the computer age, Radio Sci. Bull., 305 (2003), pp. 30–37.

[29] Z. XU AND W. CAI, Fast analytical methods for macroscopic electrostatic models in biomolecular simulations, SIAM Rev., 53 (2011), pp. 683–720, http://dx.doi.org/10.1137/090774288.

[30] L. POLADIAN, General theory of electrical images in sphere pairs, Quart. J. Mech. Appl. Math., 41 (1988), pp. 395–417, http://dx.doi.org/10.1093/qjmam/41.3.395.

[31] I. V. LINDELL, Electrostatic image theory for the dielectric sphere, Radio Sci., 27 (1992), pp. 1–8, http://dx.doi.org/10.1029/91RS02255.

[32] Z. GAN, H. WU, K. BARROS, Z. XU, AND E. LUIJTEN, Comparison of efficient techniques for the simulation of dielectric objects in electrolytes, J. Comput. Phys., 291 (2015), pp. 317–333, http://dx.doi.org/10.1016/j.jcp.2015.03.019.

[33] K. F. FREED, Perturbative many-body expansion for electrostatic energy and field for system of polarizable charged spherical ions in a dielectric medium, J. Chem. Phys., 141 (2014), 034115, http://dx.doi.org/10.1063/1.4890077.

[34] R. J. TOUGH AND A. J. STONE, Properties of the regular and irregular solid harmonics, J. Phys. A, 10 (1977), pp. 1261–1269, http://dx.doi.org/10.1088/0305-4470/10/8/004.

[35] L. GREENGARD, The Rapid Evaluation of Potential Fields in Particle Systems, MIT Press, Cambridge, MA, 1987.

[36] O. D. KELLOGG, Foundations of Potential Theory, Dover, New York, 1953.

[37] P. R. WALLACE, Mathematical Analysis of Physical Problems, Dover, New York, 1984.

[38] W. CAI, S. DENG, AND D. JACOBS, Extending the fast multipole method to charges inside or outside a dielectric sphere, J. Comput. Phys., 223 (2007), pp. 846–864, http://dx.doi.org/10.1016/j.jcp.2006.10.019.

[39] L. F. A. ARBOGAST, Du calcul des dérivations, Levrault, Strasbourg, 1800.

[40] L. C. BIEDENHARN, J. D. LOUCK, AND P. A. CARRUTHERS, Angular Momentum in Quantum Physics: Theory and Application, Addison–Wesley, Reading, MA, 1981.

[41] Z. GIMBUTAS AND L. GREENGARD, Fast multi-particle scattering: A hybrid solver for the Maxwell equations in microstructured materials, J. Comput. Phys., 232 (2013), pp. 22–32, http://dx.doi.org/10.1016/j.jcp.2012.01.041.

[42] A. J. HESFORD, J. P. ASTHEIMER, L. GREENGARD, AND R. C. WAAG, A mesh-free approach to acoustic scattering from multiple spheres nested inside a large sphere by using diagonal translation operators, J. Acoust. Soc. Am., 127 (2010), pp. 850–861, http://dx.doi.org/10.1121/1.3277219.

[43] FMMLIB3D software suite, http://www.cims.nyu.edu/cmcl/fmm3dlib/fmm3dlib.html.